Field Experiments in the Control of a Jellyfish Tracking ROV

Jason Rife and Stephen M. Rock
Stanford University, CA 94305
and Monterey Bay Aquarium Research Institute, Moss Landing, CA, 95039
Email: {jrife,rock}@arl.stanford.edu

***Abstract*—Continuing ocean experiments demonstrate specific applications in which a jelly-tracking ROV pilot assist enhances collection of scientific data. Recent results have repeatedly demonstrated the tracker's ability to follow a jelly target for extended periods, as long as 34 minutes. Thus far, experimental demonstrations of the jelly tracker have incorporated a linear control law. This paper presents extensions to the control law that enable two new capabilities. The first extension compensates for steady ROV disturbances. The second extension gives pilots full authority in the null space of the jelly tracking regulation law. Bias compensation serves to smooth transition from human pilot to combined computer-human control and to establish a clear zero reference for supplementary pilot commands issued during tracking. Use of the regulator null space enables the pilots to view the target from multiple angles.**

NOMENCLATURE

$\{x, y, z, \psi\}$	Set of Cartesian coordinates describing translation and yaw rotation (about gravity vector)
$\{r, \gamma, z, \psi\}$	Set of cylindrical coordinates describing radius, circumferential angle, depth, and yaw angle
${}^k p_l \in \mathbb{R}^4$	Position vector expressed in the reference frame and coordinate system k that describes the location and yaw orientation of the frame l
${}^k S_m\left({}^k p_l\right)$	Transformation of position vector ${}^k p_l$ to ${}^m p_l$
${}^k q_l \in \mathbb{R}^n$	Vector describing states expressed in reference frame k and used for estimation or control of an object with the attached frame l
${}^k u \in \mathbb{R}^4$	Control input, expressed in k
${}^k A \in \mathbb{R}^4$	Acceleration of frame k relative to inertial frame
${}^k D \in \mathbb{R}^4$	Vehicle drag in k
${}^k T \in \mathbb{R}^4$	Tether tension in k
${}^k \tau \in \mathbb{R}^4$	Vehicle thrust in k
${}^k F \in \mathbb{R}^4$	Force bias on ROV in k
${}^k m \in \mathbb{R}^{4x4}$	Diagonal mass and inertia matrix, including added mass, in k
${}^k b \in \mathbb{R}^{4x4}$	Diagonal drag coefficient matrix, in k
${}^k \alpha \in \mathbb{R}^{4x4}$	Diagonal thruster coefficient matrix, in k
	Reference frames (k,l):
j	Jelly centered frame, Cartesian coordinates
c	Jelly centered frame, cylindrical coordinates
v	Vehicle frame, Cartesian coordinates
r	Inertial frame aligned with vehicle coordinates
w	Inertial world frame

I. INTRODUCTION

Ocean experiments, performed in conjunction with the Monterey Bay Aquarium Research Institute (MBARI), have demonstrated the utility and feasibility of automation that assists human pilots in tracking gelatinous marine animals. As a fundamental goal, the jelly-tracking system seeks to extend the duration for *in situ* observation of marine animals. From an operational standpoint, the system addresses a limitation critical to long duration observation: pilot fatigue. By freeing the pilot from the continuous strain of the regulation task, the jelly-tracking system can deliver the capability for long term observation of a single specimen living in its native ocean habitat.

To hold station on a gelatinous target, one of the fundamental challenges lies in sensing. Previous papers describe a visual sensing system appropriate for the jelly-tracking task [1,2]. The system employs vision processing techniques to detect the target in real time despite unfavorable conditions associated with ocean imaging, including uneven lighting, marine snow, and the presence of multiple animals in the video sequence. Three extended jelly tracking experiments, with durations as long as 34 minutes, successfully demonstrated the visual sensing system in the open ocean. Of the three tracking experiments, two were terminated by the decision of the ROV pilot; one terminated as the result of a recognition failure by the vision system.

The experimental jelly-tracking system uses a linear law for feedback control.

This paper modifies the jelly-tracking controller to enable two new capabilities. First, the enhanced controller cancels out bias disturbances on the submersible to smooth transition to combined human-computer control. Also, the modified law enables pilots to issue large commands in the regulation law null space. These two capabilities fall under the umbrella of shared control, a topic concerned with the merging of multiple controllers, both automated and human.

Section II reviews the jelly-tracking system used in ocean trials, its linear control law, and the results of recent ocean experiments with MBARI *ROV Ventana.* The remainder of the paper examines extensions to the fielded system intended to improve interaction between automation and human control. Section III presents the ROV dynamic equations. Section IV proposes an estimator, based on these dynamic equations, which can smooth transition during system initialization. Section V proposes a control framework that allows the human pilot to command large motions in the regulation law null space.

II. JELLY TRACKING EXPERIMENTS

A. Experimental Hardware

Field experiments were conducted with the *ROV Ventana*, a tethered, unmanned research submersible of approximately three tons, shown in Figure 1. Three hydraulic thruster pairs (fore-aft, lateral, and vertical) actuate the vehicle in the three translational degrees of freedom. Differential actuation of the fore-aft thrusters moves the vehicle in a fourth degree of

Figure 1. *ROV Ventana*

freedom, yaw rotation. Pitch and roll rotations are passively stabilized by a buoyancy moment. Vehicle pitch and roll angles generally remain less than three degrees from neutral throughout ocean testing.

Stereo vision serves as the primary vehicle sensor, measuring target position relative to the ROV. Two stereo systems have been tested. The first uses the main science camera and an auxiliary camera, each mounted on its own pan-tilt unit, with a baseline separation of approximately one meter. The second system uses parallel stereo cameras both mounted on the same pan-tilt unit and separated by a baseline of ten centimeters. Pan-tilt units are not connected to the automated control system and can be adjusted only by the human pilot. The jelly-tracking computer, located in the control room of the support vessel, uses vision processing to determine the location of the target in each video frame and uses triangulation to give an approximate measurement of target relative location. Details regarding the vision processing algorithm are described in [1].

A control law, implemented on the jelly-tracking computer, maps the target's relative position to a thruster output. The subsequent section describes the control laws used by the fielded system.

Communication links between the jelly-tracking computer and other system components are summarized with a block diagram in Figure 2. Thruster commands are sent from the jelly-tracking computer via a serial link to the ROV control computer, which sums automated and human pilot commands. Summed commands are then sent via a 2000 m umbilical to the ROV. When sensor data return from the submersible to the surface ship, the ROV control computer routes relevant information back to the jelly-tracking computer. This signal includes measurements of the total control output (computer plus pilot), the vehicle's compass heading, and the vehicle's pressure depth. Serial communication occurs at 10 Hz, sufficiently faster than the closed loop vehicle bandwidth such that discrete control effects may be neglected.

B. Linear Control Law

The jelly-tracking system used for field trials to date relies on a linear control law. The state vector for the control law describes the ROV's position and velocity in a cylindrical coordinate system centered on the jelly target.

$$ {}^{c}q_{v} = \begin{bmatrix} \dot{r}_b & \dot{z}_b & \dot{\psi} & r_b & z_b & \psi \end{bmatrix}^{T} \qquad (1) $$

A linear proportional-derivative law with diagonal gain matrices, K_p and K_d, provides feedback control.

$$ {}^{c}u_{c} = -\begin{bmatrix} K_d & K_p \\ 0 & 0 \end{bmatrix} {}^{c}q_{v} \qquad (2) $$

The control law is based on the assumption of a system locally linear for small motions about the regulation reference point. Control gains were estimated from an approximate system model and tuned in the field. The law assumes neutral vehicle buoyancy, minimal tether forces, and minimal jelly acceleration relative to the inertial frame.

C. Endurance Testing

The jelly-tracking system was tested in the Monterey Bay with MBARI *ROV Ventana*. Successful long-duration tracking runs served to demonstrate applications of the jelly-tracking system. Several short (less than five minute) tracking runs were recorded. In addition, three experimental

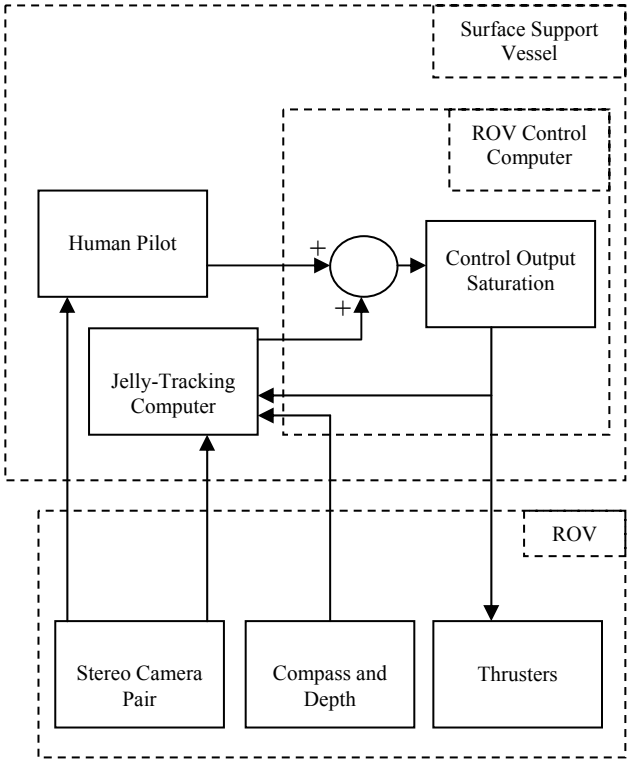

Figure 2. System block diagram

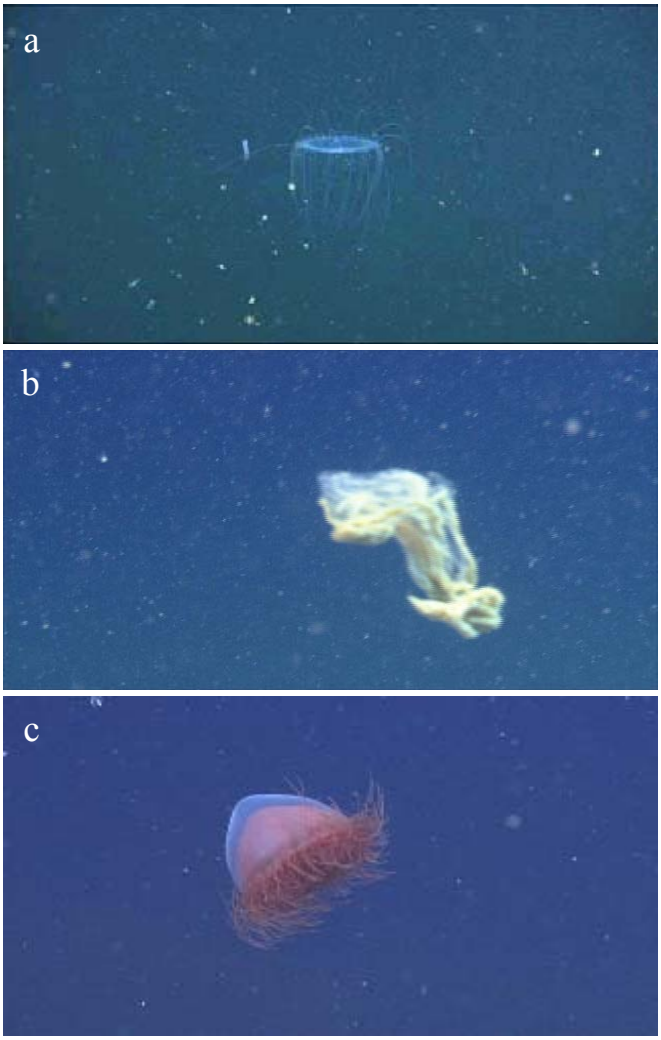

Figure 3. Three specimens tracked for an extended duration: (a) *Solmissus*, (b) Larvacean house, (c) *Benthocodon*.

trials, from two distinct dive dates, were allowed to run for longer periods of time. These extended tracking runs, of which the longest endured over 34 minutes, are summarized in Table 1 and Figure 3. Only one of the three runs listed in the table was terminated as a result of a tracking system failure; the other two would have continued longer if not for operational concerns described in the table.

The second tracking run, involving a sinking larvacean house, repeated a specific experiment described by Hamner and Robison [3]. The larvacean *Bathochordaeus*, not a true jellyfish but a gelatinous Urochordate, builds and then sheds a feeding filter, known commonly as its "house." The larvacean periodically abandons and rebuilds its house. The old filter, laden with oversize particulates, descends toward the ocean floor. Hamner and Robison measured sinking rates for larvacean houses and hypothesized that the flux of these houses serves as an important mechanism providing nutrients to bottom dwelling species. Figure 4 presents data from a series of eight larvacean tracking runs measured by Hamner et al. with the *ROV Venana* piloted under human control.

The same figure also plots data from the automated larvacean house tracking experiment. The depth trace taken

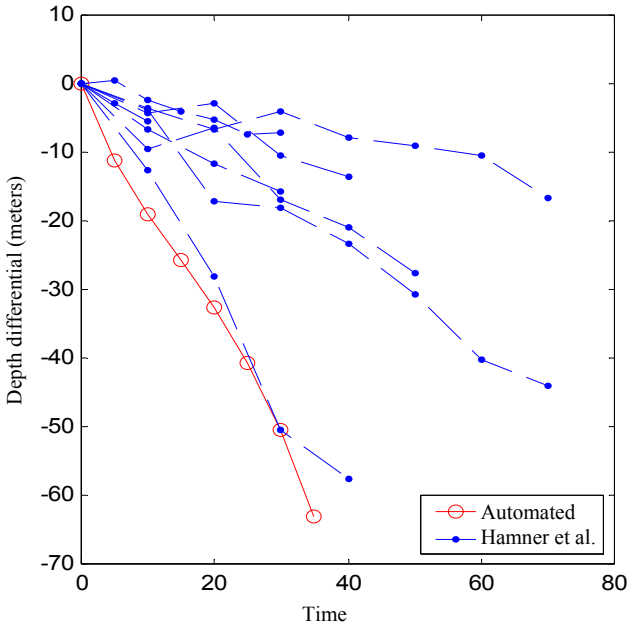

Figure 4. Traces of depth differential against time for descending larvacean house. Data captured during an automated jelly-tracking dive is plotted alongside data captured manually and reported by Hamner.

during the automated experiment (average velocity 2.4 km/day) aligns qualitatively with the descent of the fastest of the eight larvacean houses measured by Hamner (average velocity 2.1 km/day). Hamner's paper attributes the speed of the fastest of the eight samples to its "arrow-shaped, streamlined" form, a description which applies equally well to the rapidly descending house tracked by the automated pilot assist.

The demonstration reproduces a science result, and shows that automation could aid in acquiring the large quantity of additional data required to make conclusions about the ecological impact of falling larvacean houses. Other potential applications for the jelly-tracking system include making quantitative *in situ* measurements of jelly motion relative to the water column and enabling production of high quality scientific movies through ROV stabilization.

D. Extensions to the Core Jelly-tracking System

Balancing the roles of human and automated operators remains an open research area. In the case of the jelly-tracking pilot assist, introducing automation serves to reduce operator fatigue and to free the operator to make higher level supervisory decisions. This work makes no attempt,

Table 1. Description of three extended tracking experiments conducted in the open ocean with *ROV Ventana*

Animal Tracked	Tracking Duration (min)	Run Termination
Solmissus	24.5	Loss of vision lock – recognition failure
Larvacean house	34.2	Larvacean house arrives at ocean floor
Benthocodon	29.4	Support ship recalls ROV

however, to remove the human pilot completely from the control loop. In most complex systems, increased automation beyond a critical threshold yields diminishing returns. In ROV operations on the open ocean, the human pilot plays an important role in a myriad of higher level navigation and control functions, in image interpretation, in fault tolerance, and in tether management. For the jelly-tracking task, the human pilot also serves an important role in locating and identifying the target and in holding station on the jelly during initialization of the visual sensor.

The importance of the pilot in overall vehicle management means that the pilot must maintain control authority at all times. As a result, the jelly-tracking pilot assist must be considered as an element of a shared control system that combines both human and automated controllers. This paper discusses two improvements to the basic jelly-tracking system designed to enhance interaction between the automated system and the human pilot.

The first modification involves cancellation of bias disturbances on the jelly-tracking ROV. Strong bias forces, caused primarily by tether tension, are frequently observed in ocean operations. During a high-wind dive in May 2002, bias forces were measured consistently near 60% of the thruster's saturation output. With an estimator added to the tracking system, the system can infer the bias force during the initialization phase for the visual sensor. The estimated bias force can then be countered by the controller, permitting smoother transition to automatic jelly tracking and establishing a zero reference for pilot stick commands issued during tracking.

A second modification alters the linear control law described in Section II.B to compensate for a class of large motion commanded by the human pilot. Pilots routinely circle around a target jelly for data collection or for scientific filming. Using the null space of the regulation law provides the human pilot the opportunity to issue certain commands without having to fight a restoring control force. A reformulation of the vehicle control law is required, however, to open the null space to the human pilot.

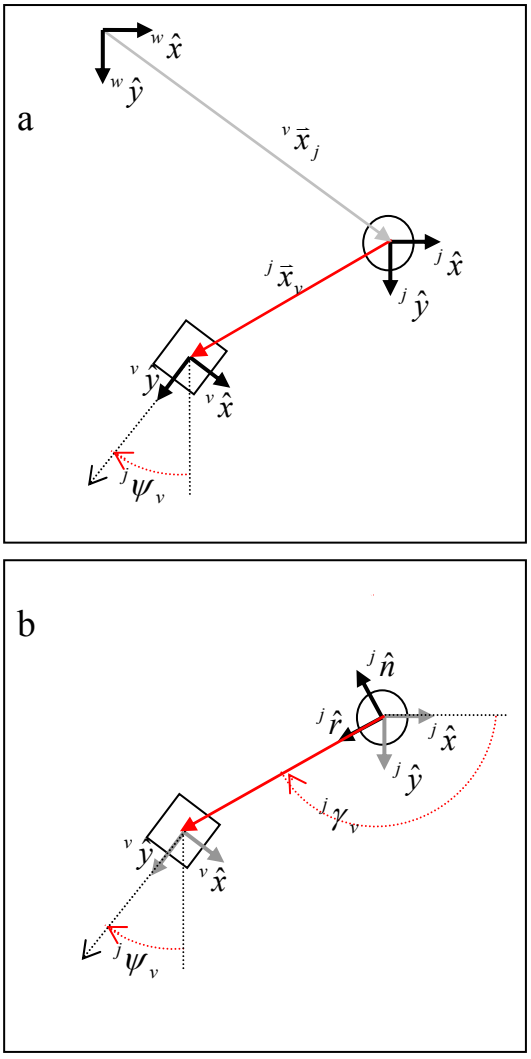

Figure 5. Jelly tracking coordinate systems: (a) Cartesian, (b) Cylindrical. A circle indicates the jelly target. A square indicates the ROV

III. ROV DYNAMIC EQUATIONS

The estimator that detects a steady bias disturbance and the control law that permits the pilot to command large null space motion both require consideration of the kinematic and dynamic equations for the ROV. Assumptions, based on empirical observations during field experiments, are introduced to reduce the dynamic and kinematic equations to the simplest possible forms that retain the functionality required for the application.

The kinematic terms in the equation of motion depend strongly on choice of reference frames. Figure 5 shows the two coordinate systems used in this paper to describe ROV position relative to the target. Both systems neglect pitch and roll motions, which remain small for large ROVs stabilized by buoyancy. The first system, *j*, uses Cartesian coordinates centered on the target jelly to describe a vehicle position vector, ${}^{j}p_{v}$. The second system, *c*, instead uses cylindrical coordinates, also centered on the target jelly, to describe a vehicle position vector, ${}^{c}p_{v}$.

$$ {}^{j}p_{v} = \begin{bmatrix} {}^{j}x_{v} & {}^{j}y_{v} & {}^{j}z_{v} & {}^{j}\psi_{v} \end{bmatrix}^{T} \tag{3} $$

$$ {}^{c}p_{v} = \begin{bmatrix} {}^{c}r_{v} & {}^{c}\gamma_{v} & {}^{c}z_{v} & {}^{c}\psi_{v} \end{bmatrix}^{T} \tag{4} $$

As indicated in Figure 5, the frame *j* centered on the target jelly translates with the animal. The frame does not, however, rotate relative to the inertial frame *w*. This choice of coordinate systems is consistent with the stereo vision sensor, which measures relative position between vehicle and target. Neither absolute position nor target orientation are observable from the stereo vision package. Vehicle angle sensors, including compass and inclinometers, instead measure vehicle attitude relative to the inertial frame.

In Cartesian coordinates, the vehicle equations of motion are given by (5).

$$ {}^{j}m\,{}^{j}\ddot{p}_{v} = {}^{j}T - {}^{j}D + {}^{j}\tau - {}^{j}m\,{}^{j}A \tag{5} $$

This vector statement of Newton's second law includes tether tension, drag, and thruster terms, along with a term, ${}^{j}A$, due to the acceleration of the non-inertial jelly frame, *j*, relative to the world frame, *w*.

$$ {}^{j}A = \begin{bmatrix} {}^{w}\ddot{x}_j & {}^{w}\ddot{y}_j & {}^{w}\ddot{z}_j & 0 \end{bmatrix}^T \tag{6} $$

Experimental results indicate that a linear law adequately describes drag for the ROV system, even for large motions away from a reference location. Accepting a linear drag law, the total vehicle drag, ${}^{j}D$, can be decomposed into two linear terms, according to (7). The equation combines one term expressing vehicle velocity relative to the jelly and a second term expressing jelly velocity relative to the water. Assuming constant water velocity local to the jelly, the water frame is identical to the inertial world frame, *w*.

$$ {}^{j}D = {}^{j}b\left({}^{w}\dot{p}_j + {}^{j}\dot{p}_v \right) \tag{7} $$

Whereas the velocity of the ROV relative to the jelly, ${}^{j}\dot{p}_v$, can be measured directly, the velocity of the jelly relative to the surrounding water, ${}^{w}\dot{p}_j$, cannot be measured with the existing jelly-tracking system. Ocean observation, however, supports a quasi-static assumption that target velocity remains constant. Jellies commonly found in the Monterey Bay (i.e. *Solmissus, Mitrocoma, Colobonema*) appear to remain motionless for minutes at a time. When these jellies begin to swim, they travel at a cruising velocity, with small periodic variations caused by pulsations of the jelly's bell. Assuming constant jelly swimming velocity implies that the associated drag term, ${}^{j}b\,{}^{w}\dot{p}_j$, remains constant and that the jelly acceleration term, ${}^{j}A$, is zero.

Based on field observations, tether tension can also be treated as an approximately constant vector disturbance. The assumption implies that the tether is always in tension and does not slack. This implication adequately describes jelly-tracking applications, as MBARI operates *ROV Ventana* with a neutrally buoyant tether that does not snap between tension and slack loads under sea states typically encountered during a research dive. The magnitude of the tether tension bias disturbance is particularly high, however, on windy days as the velocity differential between the ocean surface and ocean depths exerts a drag along the ROV tether.

With tether tension and vehicle drag associated with the jelly swimming velocity assumed quasi-steady, the two terms can be lumped into a combined force disturbance. This term, ${}^{j}F$, is observable using an estimator, as described in the following section.

$$ {}^{j}F = {}^{j}T - {}^{j}b\,{}^{w}\dot{p}_j \tag{8} $$

Equation (9) synthesizes these assumptions concerning forces on the ROV to give a new set of observable and approximate vehicle dynamic equations.

$$ {}^{j}m\,{}^{j}\ddot{p}_v + {}^{j}b\,{}^{j}\dot{p}_v = {}^{j}F + {}^{j}\tau \tag{9} $$

This equation is incorporated into the estimation law presented in the following section. For control, however, a cylindrical coordinate system more naturally decouples the regulation range and null spaces. The transformation of (9) into a jelly centered cylindrical coordinate system, *c*, produces (10).

$$ {}^{c}\ddot{p}_v = {}^{j}S_c \left({}^{j}m \right)^{-1} \left({}^{j}F - {}^{j}b\,{}^{j}\dot{p}_v + {}^{j}\tau \right) + {}^{c}A \tag{10} $$

The cylindrical equation includes the transformation matrix ${}^{j}S_c$.

$$ {}^{j}S_c = \begin{bmatrix} \cos\left({}^{c}\gamma_v\right) & -\sin\left({}^{c}\gamma_v\right) & 0 & 0 \\ \left({}^{c}r_v\right)^{-1}\sin\left({}^{c}\gamma_v\right) & \left({}^{c}r_v\right)^{-1}\cos\left({}^{c}\gamma_v\right) & 0 & 0 \\ 0 & 0 & 1 & 0 \\ 0 & 1 & 0 & 1 \end{bmatrix} \tag{11} $$

Curvilinear accelerations due to the cylindrical coordinate transformation are expressed by the term ${}^{c}A$ in (10).

$$ {}^{c}A = \begin{bmatrix} {}^{c}r_v \left({}^{c}\dot{\gamma}_v \right)^2 & -2\,{}^{c}\dot{\gamma}_v\,{}^{c}\dot{r}_v\,{}^{c}\left(r_v\right)^{-1} & 0 & -{}^{c}\ddot{\gamma}_v \end{bmatrix}^T \tag{12} $$

So that the control reference for the vehicle yaw angle, ${}^{c}\psi_v$, is zero when the vehicle points at the target jelly, (${}^{v}\hat{x} = -{}^{j}\hat{r}$), the position of the vehicle in cylindrical coordinates is defined with an offset according to (13).

$$ {}^{c}p_v = {}^{j}S_c\,{}^{j}p_v + \begin{bmatrix} 0 & 0 & 0 & \pi \end{bmatrix}^T \tag{13} $$

To improve control law performance further, a thruster model should be included with the vehicle dynamic equations. A first-order linear thruster model adequately captures the relation between control input and thruster output. Linear lead compensation may be used to handle thruster lag effects, as suggested by Yoerger et al. [4].

$$ {}^{v}\dot{\tau} = \alpha\left({}^{v}u - {}^{v}\tau \right) \tag{14} $$

For higher performance requirements, a physics based thruster model could also be introduced [4-7]. Control based on these thruster models requires additional sensing (i.e. thruster load cells or encoders). Consideration of nonlinear thruster dynamics becomes particularly important if limit cycles degrade control law performance. Limit cycles do not appear, however, when a bias force offsets from zero the equilibrium thrust required to hold station.

IV. ESTIMATION

A. Estimator

An estimator serves an important role in observing the bias disturbance on the ROV. A modified controller can apply a thrust bias to counteract the estimated disturbance. Bias force subtraction enables smooth transition to combined human computer control. Also, bias subtraction provides the human pilot with a clear zero reference for command inputs superposed on the automated regulation law.

This estimator based approach to bias subtraction serves a function similar to integral control action. The estimator based approach is more appropriate for a shared control system because it is insensitive to the source of the control command: human, computer, or shared. This characteristic occurs because the estimator employs a vehicle model and measurements of the actual control signal sent to the ROV thrusters. A related advantage of the estimator based approach results from the fact that the estimator incorporates no notion of a reference location. If the human pilot wishes to introduce a steady state tracking error, the bias estimation approach does not seek to erode this error, as an integral controller would.

In addition to its role in offsetting the bias force in a shared control system, the estimator is used to infer vehicle velocity and thruster states from a sensing system that detects vehicle relative position, only.

Estimation relies on the dynamic equations for the jelly-tracking apparatus. The system given by the vehicle and thruster equations of motion, (9) and (14), is linear and thus a linear estimation filter may be implemented for the present application. If higher precision thruster, drag, or tether models were required for accurate tracking, a nonlinear estimation technique, such as the extended Kalman filter, would instead be substituted for the linear estimator.

System linearity depends on one further assumption in addition to those described in Section III. The assumption holds that added mass and vehicle drag coefficient are uniform around the ROV's yaw axis. For open frame ROVs with no streamlining the assumption is reasonable.

$$\begin{aligned} b &= {}^{j}b = {}^{c}b = {}^{v}b \\ m &= {}^{j}m = {}^{c}m = {}^{v}m \end{aligned} \tag{15}$$

As written the thruster equation (14) uses thrust in the vehicle frame, ${}^{v}\tau$, and not in the jelly frame, ${}^{j}\tau = {}^{j}S_{v}^{-1}\,{}^{v}\tau$. The appropriate transformation that unites the coordinate systems of the vehicle and thruster dynamic equations is given by (16).

$${}^{j}S_{v} = \begin{bmatrix} \cos\left({}^{j}\psi_{v}\right) & -\sin\left({}^{j}\psi_{v}\right) & 0 & 0 \\ \sin\left({}^{j}\psi_{v}\right) & \cos\left({}^{j}\psi_{v}\right) & 0 & 0 \\ 0 & 0 & 1 & 0 \\ 0 & 0 & 0 & 1 \end{bmatrix} \tag{16}$$

If (14), (15), and (16) are substituted into (9) to give (17), the results is clearly nonlinear as ${}^{j}S_{v}$ is a function of the state variable, ${}^{j}p_{v}$.

$$m\,{}^{j}\ddot{p}_{v} + b\,{}^{j}\dot{p}_{v} = {}^{j}F + \left({}^{j}S_{v}\right)^{-1}\,{}^{v}\tau \tag{17}$$

Linearity of the estimator is maintained, however, if estimated quantities are instead transformed into an inertial coordinate system, *r*, that instantaneously aligns with the rotating coordinate system, *v*. A new inertial frame *r* is chosen at each successive instant to match the time-varying frame *v*.

$${}^{r}S_{v} = {}^{j}S_{v}(t) \tag{18}$$

Transforming (17) into the *r* frame produces the coordinate set (19) and dynamic equation (20).

$${}^{r}p_{v} = {}^{j}S_{v}\,{}^{j}p_{v} \tag{19}$$

$$m\,{}^{r}\ddot{p}_{v} + b\,{}^{r}\dot{p}_{v} = {}^{r}F + {}^{v}\tau \tag{20}$$

The combination of (14) and (20) gives a linear state space description of the system with state vector, ${}^{r}q_{v}$.

$$\begin{aligned} {}^{r}\dot{q}_{v} &= \mathcal{A}\,{}^{r}q_{v} + \mathcal{B}\,{}^{v}u \\ {}^{r}p_{v} &= C\,{}^{r}q_{v} \end{aligned} \tag{21}$$

$${}^{r}q_{v} = \begin{bmatrix} {}^{r}p_{v} & {}^{r}\dot{p}_{v} & {}^{v}\tau & {}^{r}F \end{bmatrix} \tag{22}$$

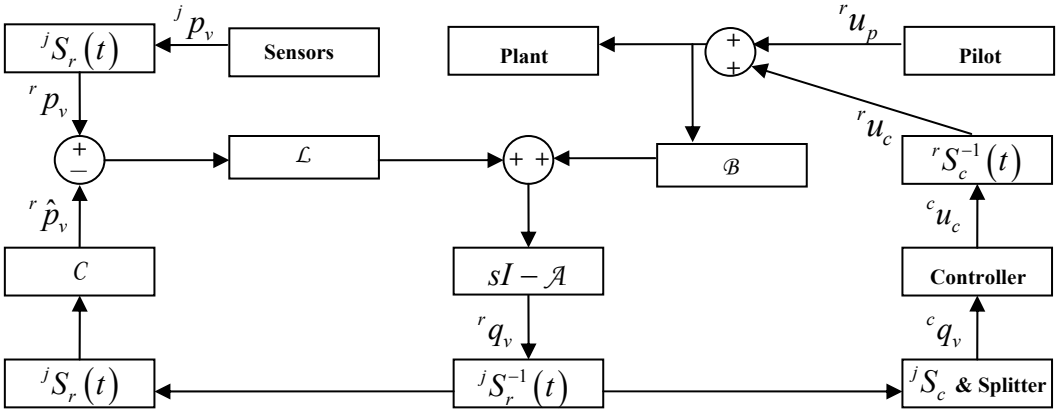

Figure 6. Block diagram for estimation

The system is described by the following matrices.

$$\mathcal{A} = \begin{bmatrix} I & 0 & 0 & 0 \\ 0 & -m^{-1}b & m^{-1} & m^{-1} \\ 0 & 0 & -\alpha & 0 \\ 0 & 0 & 0 & 0 \end{bmatrix}$$

$$\mathcal{B} = \begin{bmatrix} 0 & 0 & \alpha & 0 \end{bmatrix}^T \tag{23}$$

$$C = \begin{bmatrix} I & 0 & 0 & 0 \end{bmatrix}$$

Design of a linear estimator relies on system (23) and an approximation of process and sensor noise. Because the matrices m, b, and α are assumed diagonal, the estimator can, in fact, be designed separately for each of the four coordinate directions in the vector ${}^{r}p_v$, namely for each of three translational directions and for the yaw coordinate. To prevent coordinate system drift relative to the absolute yaw measurement, the estimated states, with the exception of the thruster states, must be converted back to the jelly coordinate system, j, after each measurement update. Figure 6 depicts a block diagram for the estimator and associated frame transformations.

V. CONTROL

A. Control Law

Enabling large pilot motions in a shared control system requires that the vehicle control law be written in a way that clearly expresses its null space. The regulation law null space results from a surplus actuated degree of freedom. Although the ROV possesses four actuated degrees of freedom, the control law that holds position relative to a target animal requires actuation in only three of these directions. The extra degree of freedom forms the basis of a control null space of order one.

The practical design of the sensing hardware places a restriction on the choice of range space coordinates. Specifically, the limited camera field of view implies that the camera's optical axis must be approximately aligned with the target animal. This restriction in turn requires that vehicle yaw and depth be regulated relative to the jelly target. A natural choice for the third range space coordinate is distance to target. Together, these three coordinates describe vehicle position in a cylindrical coordinate system. The circumferential coordinate describes the null space.

Transformation of the vehicle equations of motion to cylindrical coordinates introduces nonlinearities, as given by (10). The nonlinear system takes an affine form in terms of the thrust input, ${}^{c}\tau$.

$${}^{c}\dot{q}_v = f({}^{c}q_v, {}^{j}F) + g({}^{c}q_v)\,{}^{c}\tau \tag{24}$$

$$f({}^{c}q_v) = \begin{bmatrix} I \\ (\sigma m)^{-1}\,{}^{j}S_c\left({}^{j}F - b\,{}^{j}\dot{p}_v\right) + (\sigma)^{-1}\,{}^{c}\tilde{A} \end{bmatrix} \tag{25}$$

$$g({}^{c}q_v) = \begin{bmatrix} 0 \\ (\sigma m)^{-1} \end{bmatrix} \tag{26}$$

The reduced state vector for control, ${}^{c}q_v$, and the bias force term, ${}^{j}F$, are taken as the output of the estimator from Section IV.

$${}^{c}q_v = \begin{bmatrix} {}^{c}p_v & {}^{c}\dot{p}_v \end{bmatrix} \tag{27}$$

The cylindrical thrust vector, ${}^{c}\tau$, is the transformation of the thrust vector in the vehicle frame, ${}^{v}\tau$.

$${}^{c}\tau = {}^{j}S_c\left({}^{j}S_v\right)^{-1}\,{}^{v}\tau \tag{28}$$

Also, the curvilinear acceleration vector, given originally by equation (12), is modified to eliminate the linear component, ${}^{c}\ddot{\gamma}_v$. Shifting this component to the left hand side introduces the transformation matrix, σ, and the modified curvilinear acceleration vector, ${}^{c}\tilde{A}$.

$$\sigma = \begin{bmatrix} 1 & 0 & 0 & 0 \\ 0 & 1 & 0 & 0 \\ 0 & 0 & 1 & 0 \\ 0 & 1 & 0 & 1 \end{bmatrix}^T \tag{29}$$

$${}^{c}\tilde{A} = \begin{bmatrix} {}^{c}r_v\left({}^{c}\dot{\gamma}_v\right)^2 & -2\,{}^{c}\dot{\gamma}_v\,{}^{c}\dot{r}_v\,{}^{c}\left(r_v\right)^{-1} & 0 & 0 \end{bmatrix}^T \tag{30}$$

If the coriolis and centrifugal accelerations of (30) remain small, a linear control law can be written based on (24) that incorporates a bias subtraction term, where the bias force is projected into the cylindrical reference frame via $(\sigma m)^{-1}\,{}^{j}S_c$. In addition to bias force compensation, this linear control law differs from (2) in that the yaw regulation command must take into account a pilot command in the circumferential direction, according to (29).

If centrifugal forces are significant, a feedback linearization law, (31), can be written based on the canonical affine form of (24). The feedback linearization term, τ_{fb}, complements the desired control law, ${}^{c}\tau_{des}$,which is designed using classical linear techniques.

$$\begin{aligned} {}^{c}\tau &= {}^{c}P_\gamma\left({}^{c}\tau_{des} + \tau_{fb}\right) \\ \tau_{fb} &= -\left(\tilde{\sigma}\right)^{-1}\,{}^{j}S_c\left({}^{j}F - {}^{j}b\,{}^{j}\dot{p}_v\right) - m\left(\tilde{\sigma}\right)^{-1}\left({}^{c}\tilde{A}\right) \end{aligned} \tag{31}$$

In the feedback control expression, (31), the projection operator, ${}^{c}P_\gamma$, forces the circumferential control term to zero to enforce the notion of the circumferential null space.

$${}^{c}P_\gamma = \begin{bmatrix} 1 & 0 & 0 & 0 \\ 0 & 0 & 0 & 0 \\ 0 & 0 & 1 & 0 \\ 0 & 0 & 0 & 1 \end{bmatrix} \tag{32}$$

Thruster dynamics have not, thus far, been incorporated in the control law. To produce a practical control signal, the appropriate thruster output, ${}^{c}\tau$, must be first transformed to the vehicle reference frame using the inverse of (28). The signal can then be passed through a lead filter designed to match (14) in order to compensate for thruster dynamics.

B. Null Space Dynamics

The automated regulator is expected to handle basic station keeping tasks. The human pilot can, however, issue arbitrary commands in the circumferential null space at the same time the automatic system regulates range, depth, and bearing relative to the target.

Free reign over the vehicle's null space coordinate permits the pilot to control the orientation of the target animal in the video data record. Compared to the computerized vision processor, the human pilot easily determines target orientation and can infer semantic components of the target, such as its organs. Thus the pilot can accomplish a higher level task requested by a scientist, for instance: "circle around the specimen to observe the contents of its stomach." This capability will be tested in future experimental dives.

Past experimental dives, described in Section II.C, employed no control in the circumferential direction, automated or human. When the bias force, ${}^{c}F$, was non-zero, however, the force served to passively stabilize the ROV's circumferential location. Analysis of the circumferential row from vector equation (24) shows how the bias disturbance acts as a restoring force in the circumferential coordinate.

$$ {}^{c}\ddot{\gamma}_{v} = m^{-1}\,{}^{j}S_{c,\gamma}\left({}^{j}F - b^{j}\dot{p}_{v}\right) + {}^{c}\tilde{A}_{\gamma} \qquad (33) $$

In (33), the subscript γ refers to the circumferential row of a matrix or vector. Taking (33) to steady state allows the acceleration term, the coriolis term, and the drag term to be neglected.

$$ 0 = \left\| {}^{j}F_{planar} \right\| \sin\left({}^{c}\gamma_{v} - {}^{c}\gamma_{F} \right) \qquad (34) $$

Here the projection of the bias force vector into the circumferential plane is written in terms of a magnitude, ${}^{j}F_{planar}$, and a direction, ${}^{c}\gamma_{F}$. Two equilibrium points result, at ${}^{c}\gamma_{v} = \left\{ {}^{c}\gamma_{F}, {}^{c}\gamma_{F} + \pi \right\}$. Only the first is stable. Thus, in the absence of a circumferential control input, the bias disturbance on the ROV stabilizes the vehicle at a specific circumferential angle relative to the jelly target.

VI. CONCLUSION

The jelly-tracking system was tested in the field using MBARI's *ROV Ventana*. Repeated field experiments demonstrated the ability of the system to regulate ROV position for periods longer than a half hour without pilot interruption. Specific tests also demonstrated the capability of the automated system to repeat a previously reported ecological experiment and to enable new scientific research. All experiments were completed using a linear control law.

To permit cancellation of the tether induced bias force, an estimator and a revised control law were introduced. Also, a modified control law permits the human pilot to superpose large amplitude control commands on top the basic regulation command. The modification exploits the null space of the tracking control law, which lies in the circumferential direction of the cylindrical coordinate system centered on the target jelly. The estimator and controller introduced in this paper are in the process of being implemented for jelly tracking experiments with *ROV Ventana*. Details of these experiments will be reported in a future paper.

Acknowledgements

We thank MBARI and Packard Foundation grants 98-3816 and 98-6228 for supporting this work.

References

[1] J. Rife and S. M. Rock, "A Pilot-Aid for ROV Based Tracking of Gelatinous Animals in the Midwater," *Proc. IEEE/MTS OCEANS 2001*, vol. 2, pp. 1137-1144, 2001.

[2] J. Rife and S. Rock. "A Low Energy Sensor for AUV-Based Jellyfish Tracking," *Proc. of the 12th International Symposium on Unmanned Untethered Submersible Technology*, August, 2001.

[3] W. Hamner and B. Robison, "*In Situ* Observations of Giant Appendicularians in Monterey Bay," *Deep-Sea Research*, vol. 39, n. 7/8, pp. 1299-1313, 1992.

[4] D. R. Yoerger, J. G. Cooke, and J.-J. E. Slotine, "The Influence of Thruster Dynamics on Underwater Vehicle Behavior and Their Incorporation into Control System Design," *IEEE J. of Oceanic Engineering*, vol. 15, 1990.

[5] A. J. Healey, S. M. Rock, S. Cody, D. Miles, and J. P. Brown, "Toward an Improved Understanding of Thruster Dynamics for Underwater Vehicles," *IEEE J. of Oceanic Engineering*, vol. 20, pp. 354-361, 1995.

[6] L. L. Whitcomb and D.R.Yoerger, "Development, Comparison, and Preliminary Experimental Validation of Nonlinear Dynamic Thruster Models," *IEEE J.l of Oceanic Engineering*, vol. 24, pp. 481-494, 1999.

[7] L. L. Whitcomb and D.R.Yoerger, "Preliminary Experiments in Model-Based Thruster Control for Underwater Vehicle Positioning," *IEEE J. of Oceanic Engineering*, vol. 24, pp. 495-506, 1999.